

## C<sub>60</sub> Fullerene Governs Doxorubicin Effect on Metabolic Profile of Rat Microglial Cells In Vitro

Yevheniia Hurmach, Mariia Rudyk,\* Svitlana Prylutska, Vasyl Hurmach, Yuriy I. Prylutsky, Uwe Ritter, Peter Scharff, and Larysa Skivka



Cite This: *Mol. Pharmaceutics* 2020, 17, 3622–3632



Read Online

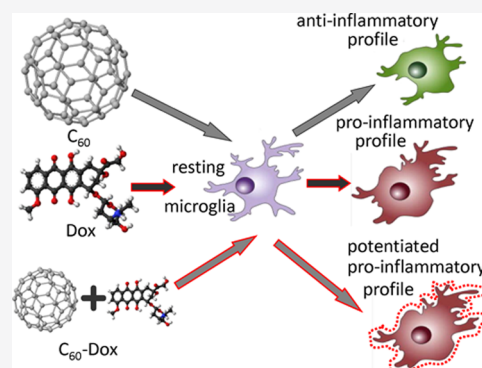
ACCESS |

Metrics & More

Article Recommendations

**ABSTRACT:** *Background:* C<sub>60</sub> fullerenes and their derivatives are actively investigated for the use in neuroscience. Applications of these nanoscale materials require the examination of their interaction with different neural cells, especially with microglia, because these cells, like other tissue resident phagocytes, are the earliest and most sensitive responders to nanoparticles. The *aim* of this study was to investigate the effect of C<sub>60</sub> fullerene and its nanocomplex with doxorubicin (Dox) on the metabolic profile of brain-resident phagocytes—microglia—in vitro. *Methods:* Resting microglial cells from adult male Wistar rats were used in experiments. Potential C<sub>60</sub> fullerene targets in microglial cells were studied by computer simulation. Microglia oxidative metabolism and phagocytic activity were examined by flow cytometry. Griess reaction and arginase activity colorimetric assay were used to explore arginine metabolism. *Results:* C<sub>60</sub> fullerene when used alone did not influence microglia oxidative metabolism and phagocytic activity but shifted arginine metabolism toward the decrease of NO generation. Complexation of C<sub>60</sub> fullerene with Dox (C<sub>60</sub>–Dox) potentiated the ability of the latter to stimulate NO generation. *Conclusion:* The capability of C<sub>60</sub> fullerenes used alone to cause anti-inflammatory shift of microglia arginine metabolism makes them a promising agent for the correction of neuroinflammatory processes involved in neurodegeneration. The potentiating action of C<sub>60</sub> fullerene on the immunomodulatory effect of Dox allows us to consider the C<sub>60</sub> molecule as an attractive vehicle for this antitumor agent.

**KEYWORDS:** C<sub>60</sub> fullerene, doxorubicin, microglia, oxidative metabolism, phagocytosis, arginine metabolism



### INTRODUCTION

The introduction of nanotechnology into neuroscience has provided extraordinary opportunities for the treatment of nervous system disorders.<sup>1</sup> Specific attention in nanoscience is given to carbon-based nanomaterials including allotropes such as fullerenes because of their ability to cross the blood–brain barrier (BBB),<sup>2</sup> to prevent neurodegeneration and protect neuroplasticity.<sup>3,4</sup> C<sub>60</sub> fullerene, as a third allotropic form of carbon, has a wide range of biological effects. C<sub>60</sub> fullerene is highly active in the soluble form when its carbon double chemical bonds are freely accessible.<sup>5</sup> The pristine C<sub>60</sub> fullerene has a very low solubility in water. However, it can form aggregates in aqueous solutions and make stable colloid solutions which contain both individual C<sub>60</sub> molecules and its nanoclusters.<sup>6,7</sup> Pristine C<sub>60</sub> fullerene aqueous colloid solution (C<sub>60</sub>FAS) is not toxic against normal cells at least at low concentrations.<sup>8,9</sup> C<sub>60</sub> fullerene being a hydrophobic molecule readily embeds into biological membranes and thus penetrates the cell.<sup>10</sup> Currently, C<sub>60</sub> fullerene and its derivatives are considered as promising therapeutic agents as well as a good candidate for drug delivery.<sup>11,12</sup> The growing number of data including our own results convincingly

shows that complexation of C<sub>60</sub> fullerene with anticancer drugs such as doxorubicin (Dox), cisplatin, and so forth significantly increases the cytotoxic effects of chemotherapeutic agents toward tumor cells.<sup>13–15</sup> In addition, conjugation of anticancer drugs with C<sub>60</sub> fullerene may help to balance severe negative side effects of chemotherapy.<sup>16</sup>

Irrespective of the location, C<sub>60</sub> fullerene unavoidably affects resident tissue macrophages, as these sentinel cells located at exposure sites are responsible for the clearance of nanoparticles.<sup>17</sup> In addition, resident macrophages are endowed with essential functions of maintaining tissue homeostasis, as well as initiating and governing immune response to foreign substances including therapeutic agents. Therefore, if and how C<sub>60</sub> fullerene and its nanocomplex with therapeutic agents would affect tissue resident macrophages need to be explored

**Received:** June 30, 2020

**Revised:** July 14, 2020

**Accepted:** July 16, 2020

**Published:** July 16, 2020



in order to create better predictive models of their therapeutic efficiency and unfavorable outcomes following exposure.

The ability of pristine  $C_{60}$  fullerenes to efficiently enter phagocytic cells through receptor-mediated endocytosis or by passive diffusion is well documented.<sup>18</sup> Several research groups reported about the prominent effect of  $C_{60}$  fullerenes on phagocyte metabolism. According to these reports, the effect depends on the baseline functional state of phagocytes:  $C_{60}$  fullerenes can induce reactive oxygen species (ROS) and Th1 cytokine expression in nonsensitized resting phagocytic cells and can inhibit ROS production as well as downregulate synthesis of proinflammatory cytokines in inflamed cells.<sup>19,20</sup> Our previous results revealed the ability of  $C_{60}$  fullerene and its nanocomplex with Dox ( $C_{60}$ -Dox) to modulate functions of resting mononuclear phagocytes inducing their ROS generation.<sup>21</sup>

Tissue-resident macrophages of different locations are characterized by a common core functional program which includes phagocytosis of pathogens and dying cells, cytokine and chemokine production, and so forth. In addition to these common features, tissue-resident macrophages of different populations have unique features and functions, which depend on the tissue in which they reside.<sup>22,23</sup> Microglial cells are the tissue-resident macrophages of the central nervous system (CNS). The recent considerable evidence indicates that microglia is a highly unique and plastic immune cell population in the CNS. These cells perform multiple functions not only in development and homeostasis of the CNS but also in aggravation of or recovery from pathological states through inflammatory and noninflammatory responses.<sup>24,25</sup> In addition, microglial cells are the major and susceptible responders to nanoparticles in the CNS.<sup>26</sup> Microglial cells, like other macrophages, are characterized by metabolic plasticity. A commonly accepted hypothesis postulates the existence of two polar activation profiles of phagocytes: M1 (classic, proinflammatory) and M2 (alternative, anti-inflammatory), whereas resting phagocytes have the M0 metabolic profile. According to this hypothesis, M1-polarized phagocytes secrete Th1 cytokines and are distinguished by the shift of arginine metabolism to upregulated inducible nitric oxide synthase (iNOS) activity with increased NO generation. M1 phagocytes participate in inflammatory processes and in antitumor immune response. M2-polarized cells release Th2 cytokines and metabolize arginine through arginase and are associated with the resolution of inflammation and tumor growth promotion.<sup>27,28</sup> However, the activation states of microglia do not fit into the paradigm of the M1/M2 macrophage dichotomy for several reasons. Microglial cells have a different developmental origin than a majority of tissue macrophages and maintain transcription profiles distinct from peripheral phagocytes. In addition, microglia in the normal, non-pathological brain exist as moderately M2-skewed population.<sup>29,30</sup> The literature data about the effect of carbon nanomaterials including  $C_{60}$  fullerene and its nanocomplex with chemotherapeutics on the metabolism of brain-resident phagocytes are sparse and controversial. It is reported that  $C_{60}$  fullerene and its derivatives can attenuate inflammatory response of BV-2 microglial cells through the downregulation of ROS generation.<sup>31,32</sup> According to the data,<sup>33</sup> electroconductive carbon nanoparticles can successively initiate the shift of microglial cell metabolism to M1 and M2 profiles in a time-dependent manner. Li *et al.*<sup>34</sup> demonstrated a high efficacy of a drug composite based on nanodiamond-bearing

Dox in the modulation of tumor-associated brain phagocyte metabolism *in vitro* and *in vivo*. Authors concluded that immunomodulatory action of these nanoformulations is one of the key components of their antitumor effect.

The aim of this study was to investigate the effect of water-soluble pristine  $C_{60}$  fullerene and its  $C_{60}$ -Dox nanocomplex on the metabolic profile of resting rat microglia *in vitro*.

## EXPERIMENTAL SECTION

**Materials and Methods.** *Preparation of  $C_{60}$ -Dox Nanocomplexes.* Highly stable  $C_{60}$ FAS (final concentration 0.15 mg/mL) used in the experiment was prepared according to the protocols developed previously.<sup>7</sup> Dox ("Dox-TEVA", Pharmachemie B.V., Utrecht, Netherlands) was dissolved in saline to obtain a final concentration of 0.15 mg/mL. It was immobilized on  $C_{60}$  fullerene according to the previously described protocol.<sup>35</sup> Briefly,  $C_{60}$ FAS (final concentration 0.15 mg/mL) and Dox (final concentration 0.15 mg/mL) were mixed in 1:2 volume ratio, and the resulting mixture was treated for 20 min in an ultrasonic disperser, and then, it was subjected to overnight magnetic stirring at room temperature.

In order to detect the complexation between  $C_{60}$  fullerene and Dox in the aqueous solution, a range of physicochemical methods such as atomic force microscopy, UV-vis, nuclear magnetic resonance, and dynamic light scattering spectroscopy were applied.<sup>35,36</sup> In particular, the small-angle neutron scattering data point out the existence of at least two statistically different entities in aqueous solution, which are the  $C_{60}$  fullerene aggregates and  $C_{60}$ -Dox nanocomplexes.<sup>37</sup> Finally, within the proposed thermodynamic model of interaction between  $C_{60}$  and Dox molecules, we calculated the equilibrium heterocomplexation constant,  $K_L \approx 60,000 M^{-1}$ .<sup>38</sup> Moreover, Dox release from the  $C_{60}$ -Dox nanocomplex was evaluated by the fluorescent-based technique.<sup>39</sup> It turned out that the content of  $C_{60}$ -Dox nanocomplexes after incubation in the RPMI culture medium for 24 h was assessed to account for  $83.83 \pm 5.47\%$  of the respective 0 h in the control.

*Molecular Docking Analysis.* For molecular docking, rigid gp91phox (PDBID 3A1F), arginase (1HQ5), iNOS (4JS9 and Q9R0W4 sequences as the template for homology modeling based on Swiss-model),<sup>40-44</sup> and  $C_{60}$  fullerene structures were used. The algorithm of systematic docking SDOCK+ was applied and<sup>45</sup> implemented in QXP<sup>46</sup> that allowed to build a possible complex of studying structures with a minimal value of root mean square deviation (RMSD).<sup>45</sup> As a result, 300 possible complexes of "protein- $C_{60}$  fullerene" were generated, out of which 10 best complexes were selected using a scoring function built-in the QXP package<sup>46</sup> for the next stages of calculation. The interaction of the gp91phox molecule with  $C_{60}$  fullerene was characterized by following parameters: (1) the number of hydrogen bonds, (2) the area of contacting surfaces, and (3) the distance between docked structures.

*Molecular Dynamics Simulation.* To evaluate the stability of the obtained "protein- $C_{60}$  fullerene" complexes after molecular docking, molecular dynamics (MD) simulation was performed using gromacs 5.1.3<sup>47</sup> in force field Charmm36.<sup>48</sup> The protein molecule was protonated in accordance to the implemented function in gromacs 5.1.3 (-ingh). The topology for  $C_{60}$  fullerene was generated by SwissParam.<sup>49</sup> A "protein- $C_{60}$  fullerene" complex was placed in the center of periodic cubic box, which was filled with TIP3P water molecules. The distance between the complex

and the edge of box was 0.9 nm. So, an investigated complex can fully contact with water and rotate freely. To neutralize the system electrostatically and imitate the cellular environment,  $\text{Na}^+$  and  $\text{Cl}^-$  ions were added. In this system, solvent molecules were randomly replaced with monoatomic ions. After that, the “protein- $\text{C}_{60}$  fullerene” complex’ energy was minimized. To relax the system, a steepest descent algorithm was used (the maximum number of steps was 50,000). Next, two equilibration stages were performed: *NVT* equalization lasted 100 ps and then *NPT* – 1 ns. Finally, MD simulation was performed within 25 ns at a temperature of 300 K.

**Microglial Cell Isolation.** All procedures on animals were conducted in accordance with the standards of the Convention on Bioethics of the Council of Europe’s “Europe Convention for the Protection of Vertebrate Animals” used for experimental and other scientific purposes (1997), the general ethical principles of animal experiments, approved by the First National Congress on Bioethics in Ukraine (September 2001). The current animal protocol was reviewed and approved by the Taras Shevchenko National University of Kyiv animal welfare committee according to the Animal Welfare Act guidelines. The standard protocol described by Frank<sup>50</sup> with slight modifications was used to isolate primary microglia from male Wistar rats (40–50 g). Rats were bred in the vivarium of the ESC “Institute of Biology and Medicine” of Taras Shevchenko National University of Kyiv and maintained in standard conditions. Animals were deeply anesthetized by intraperitoneal injection of 200  $\mu\text{L}$  of sodium pentobarbital (Narcoren, Pharmazeutischen Handelsgesellschaft, Germany) and transcardially perfused with ice-cold phosphate-buffered saline (PBS). The brain was rapidly removed on ice, and the hippocampus was excised and additionally perfused using PBS. The isolated brain tissue was gently triturated in ice-cold PBS supplemented with 0.2% glucose for 15 min at  $25 \pm 1$  °C using the Potter homogenizer. The tissue homogenate was filtered through a 40 nm cell strainer (BD Biosciences Discovery, USA) for additional disintegration followed by centrifugation at 350g for 10 min. The washed homogenate was then subjected to Percoll gradient centrifugation. For this purpose, the cell suspension was slurried in 1 mL of 70% isotonic Percoll solution. Then, 1 mL of 50% Percoll solution was then gently layered on top of the 70% layer, and 1 mL of PBS solution—on top of the 50% Percoll layer. The mixture was then centrifuged for 40 min at 1200g. The layer at the interface between the 70 and 50% Percoll phases which contains highly enriched microglia was pulled out, and cells were washed twice in ice-cold PBS. Purity of the isolated microglia was assessed by flow cytometry using fluorescein isothiocyanate (FITC)-conjugated mouse anti-rat CD11b (BD Pharmingen, USA) and PE-conjugated mouse anti-rat CD45 (BD Pharmingen, USA). The CD11b+CD45+ cell fraction was  $88.97 \pm 1.58\%$ . Microglial cell viability was defined using the Trypan blue exclusion test. The proportion of the viable cells was  $\geq 93\%$ .

**Isolation of Rat Peritoneal Macrophages.** Rat peritoneal macrophages (PMs) were isolated without preliminary stimulation as described earlier.<sup>51</sup> Animals were sacrificed, and PMs were harvested using PBS containing 100 U/mL of heparin. PMs were centrifuged at 300g for 5 min at 4 °C, washed twice with serum-free RPMI 1640, and resuspended in RPMI 1640 containing 10% FCS and 40  $\mu\text{g}/\text{mL}$  gentamycin.

**Immunofluorescence Labeling.** PE anti-CD80 antibodies and Alexa Fluor 647 labeled anti-CD206 antibodies (Abcam)

were used to determine the mean fluorescence intensity (MFI) of CD206 and CD80 on microglial cells and PMs. The antibodies were added (5  $\mu\text{L}$ ) to the cell samples (50  $\mu\text{L}$ ). Microglial cells and PMs were incubated for 25 min at room temperature. Cell samples were then analyzed by the FACSCalibur flow cytometer (BD Biosciences, San Jose, CA, USA). The data were analyzed using CELLQuest software (BD; Franklin Lakes, NJ, USA).

**Cell Incubation with  $\text{C}_{60}$  Fullerene, Dox, and  $\text{C}_{60}$ -Dox nanocomplex.** Prior to the metabolic profile examination, 200  $\mu\text{L}$  of microglial cells or PM suspension in RPMI 1640 medium was treated with  $\text{C}_{60}$  fullerene, Dox, or  $\text{C}_{60}$ -Dox nanocomplex at a concentration of 0.15 mg/mL for 30 min.

**ROS Assay.** Intracellular ROS generation was detected using carboxy-H2DCFDA (H2DCFDA, Invitrogen, USA).<sup>52</sup> Carboxy-H2DCFDA is a ROS-sensitive membrane-permeable fluorescent probe that is converted to impermeable green-fluorescent form when oxidized. Briefly,  $2 \times 10^5$  phagocytic cells were incubated with PBS containing 10  $\mu\text{mol}$  carboxy-H2DCFDA at 37 °C in the dark for 30 min. After this, fluorescence was measured using a FACScan (Becton-Dickinson, USA) at an excitation wavelength of 488 nm and an emission wavelength of 525 nm. Only viable cells, gated according to the scatter parameters, were used for the analysis. ROS levels were characterized by fluorescence intensity.

**Phagocytosis Assay.** The phagocytosis assay was performed by flow cytometry as described by Cantinieaux *et al.*<sup>53</sup> *Staphylococcus aureus* Cowan I cells (collection of the Department of Microbiology and Immunology of ESC “Institute of Biology and Medicine” of Taras Shevchenko National University of Kyiv) were grown on meat-peptone agar followed by heat inactivation and FITC labeling. The stock of FITC-labeled *S. aureus* was added to  $2 \times 10^5$  phagocytic cells at a concentration of  $1 \times 10^7$  cells/mL in a volume of 10  $\mu\text{L}$ . A sample with microglial cells without bacteria served as a negative control. All samples were incubated at 37 °C for 30 min. After the incubation, phagocytosis was stopped by the addition of cold PBS with 0.02% ethylenediaminetetraacetic acid and 0.04% paraformaldehyde. Fluorescence of phagocytes with engulfed bacteria was determined by flow cytometry. Results were registered as the percentage of phagocytizing cells and as the phagocytosis index (PI) that represent the mean fluorescence per one phagocytic cell (bacteria ingested by a single cell).

**Nitrite Assay.** Nitrite level examination was conducted to evaluate NO release into the conditioned media of phagocytic cells as described previously.<sup>54</sup> Briefly, after the treatment of cells with nanoformulations, the conditioned media were collected, and the nitrite concentration in each sample was assayed by the Griess assay. Equal volumes of 2% sulfanilamide in 10% phosphoric acid and 0.2% *N*-(1-naphthyl)-ethylenediamine dihydrochloride were mixed to prepare the Griess reagent (GR). GR (100  $\mu\text{L}$ ) was mixed with equal volumes of the supernatant directly in the wells of a 96-well plate, and the mixture was then incubated at room temperature in the dark for 30 min. The absorbance ( $\lambda = 548$  nm) of the formed chromophore was measured with a plate reader. The nitrite content was calculated with sodium nitrite as a standard for a calibration curve. Each sample was assayed in triplicates. Each value was divided by the number of viable cells and presented as nitrite level per  $10^6$  cells. The mean value and SD were calculated with normalized values.

**Arginase Activity Assay.** Arginase activity was detected in cell lysates by the standard colorimetric method with some modifications.<sup>52</sup> Briefly, the reaction mixture containing 100  $\mu\text{L}$  of 0.1% Triton X-100, 100  $\mu\text{L}$  of 50 mmol Tris-HCl (pH 7.5), and 10 mmol  $\text{MnCl}_2$  was added to cell samples. Arginase enzymatic activity was then activated by heating the phagocytic cell suspension for 7 min at 56  $^\circ\text{C}$ . The reaction of L-arginine hydrolysis by arginase was performed by incubation of the cell suspension containing activated arginase, with 100  $\mu\text{L}$  of L-arginine (0.5 M; pH 9.7) for 2 h at 37  $^\circ\text{C}$ , and was stopped by the addition of 800  $\mu\text{L}$  of the mixture of acids ( $\text{H}_2\text{SO}_4/\text{H}_3\text{PO}_4/\text{H}_2\text{O} = 1:3:7$ ). For colorimetric determination of urea,  $\alpha$ -isonitrosopropiophenone (40  $\mu\text{L}$ , 9% solution in ethanol) was added, and the mixture was incubated for 30 min at 95  $^\circ\text{C}$  and then for 30 min at 40  $^\circ\text{C}$ . The urea concentration was measured immediately on a microplate reader at  $\lambda = 540$  nm. Each experiment variant was tested in triplicates. Each value was divided by the number of viable cells and presented as urea level/h per  $10^6$  cells. The mean value and SD were calculated with normalized values.

**Statistical Analysis.** All experimental results are reported as mean  $\pm$  SD. Statistical significance of the results was determined by Student's *t*-test (unpaired, two-tailed), comparing two groups of independent samples. Means were compared, and differences were considered significant at  $p \leq 0.05$ .

## RESULTS

**Microglial Cells Exhibit Slight M2 Metabolic Skew as Compared to PMs.** Comparative analysis of phenotypic and functional characteristics of resting rat microglial cells and PMs revealed substantial differences in these two populations of tissue resident phagocytes (Table 1). In order to characterize

**Table 1. Phenotypic and Functional Characteristics of Rat Resting Microglial Cells and PMs<sup>a</sup>**

phenotypic/functional characteristic	microglia	PMs
ROS generation, GMean	75.6 $\pm$ 4.37*	389.21 $\pm$ 13.12
PI, GMean	67.5 $\pm$ 2.91*	80.1 $\pm$ 3.32
arginase activity, $\mu\text{g}$ urea/hper $10^6$ cells	0.485 $\pm$ 0.17*	0.257 $\pm$ 0.01
NO level, $\mu\text{M}/10^6$ cells	5.56 $\pm$ 0.89*	11.91 $\pm$ 1.31
CD206 expression, GMean	48.01 $\pm$ 6.13*	167.32 $\pm$ 8.19
CD80 expression, GMean	52.21 $\pm$ 0.69*	94.33 $\pm$ 5.62

<sup>a</sup>Data are represented as mean  $\pm$  SD. \*— $p \leq 0.05$  was considered significant compared with the corresponding values in the PMs.

the phenotypic phagocyte profile, we have used two markers: CD80 and CD206. CD80 (a costimulatory molecule, which plays an important role in T-cell activation) is the marker of M1 macrophage polarization.<sup>55</sup> CD206 (mannose receptor C type 1) serves as a marker to identify the M2 macrophage phenotype.<sup>56</sup> The levels of CD206 and CD80 expression were lower in microglial cells as compared to PMs. This can be explained by the unique microglia phenotype. According to the literature data, the resting adult microglia include cells, which express neither CD206 nor CD80 or express these markers at very low levels. Meanwhile, microglia activation can be associated with upregulation of both CD206 and CD80.<sup>57</sup> These results suggest that commonly used macrophage phenotypic markers CD80 and CD206 cannot effectively distinguish M1 and M2 subtype microglia, and metabolic

features could be more useful for this purpose. In our experiments, spontaneous ROS generation in microglial cells was five times lower than that in PMs. The NO level in microglia was also significantly lower than that in PMs. Meanwhile, arginase activity in microglial cells was two times higher than that in PMs. Comparative analysis of metabolic characteristics of resting tissue-resident macrophages of different locations (spleen, bone marrow, lung, and peritoneal cavity) indicates the most stable M0 functional state in PMs.<sup>58,59</sup> Taking it into account, as well as considering the fact that increased arginine metabolism through the arginase along with decreased iNOS activity is the sign of alternatively polarized (M2) phagocytes, one can suggest that resting microglial cells are characterized by a slight M2 metabolic shift as compared to PMs.

**C<sub>60</sub> Fullerene Does Not Affect Resting Microglia Oxidative Metabolism and Dox-stimulated ROS Generation.** Considering a well-documented prominent impact of C<sub>60</sub> fullerene on phagocyte oxidative metabolism,<sup>60–62</sup> we first examined the effect of C<sub>60</sub> fullerene and its nanocomplex with Dox on intracellular ROS generation in resting microglial cells. The major source of ROS in professional phagocytes such as microglial cells is a superoxide-generating NADPH oxidase. The NADPH oxidase is a multicomponent enzyme comprised of a membrane-bound heterodimer, flavocytochrome b558, which consists of a large subunit, gp91phox (NOX2), and a small subunit, p22phox, and cytosolic regulatory subunits p67phox, p47phox, p40phox, and Rac. Phagocyte NOX2 (Phox) is constitutively expressed but inactive in resting cells and is activated by the ligation of toll-like receptors (TLRs) including TLR4. Upon this condition, Phox becomes activated in the cell phagosomal membrane after ingestion of the TLR4-bound substance into the phagosome, delivering high concentrations of superoxide into this compartment, with subsequent production of additional ROS.<sup>63–65</sup> Therefore, we suggested that microglial gp91phox can be one of the important targets for C<sub>60</sub> fullerene-based nanoformulation. In our study, functional tests were preceded by molecular docking, which allow imitating the behavior of small molecules of our interest in the binding sites of microglial cells. The docking site was determined accordingly.<sup>66</sup> So, the main binding amino acids in the case of “gp91phox–C<sub>60</sub> fullerene” complex have been identified, namely Glu 156, Pro 155, Cys 153, Phe 186, Asn 185, and Lys 183. According to molecular docking, it was shown that C<sub>60</sub> fullerene sterically interacts with Pro 155, Glu 156, and Asn 185. From the other side, stacking interactions of C<sub>60</sub> fullerene with Cys 153 and Phe 186 were observed. Furthermore, there is a possibility of  $\pi$ -cation interaction between the C<sub>60</sub> molecule and Lys 183 (Figure 1A).

MD simulation has shown the stability of the “gp91phox–C<sub>60</sub> fullerene” complex: the range of movement for the gp91phox molecule was 0.12–0.33 nm and for C<sub>60</sub> fullerene was 0.24–1.12 nm (Figure 2). Despite such movement of C<sub>60</sub> fullerene, stable interactions during MD simulation were found (Figure 1B), namely, steric interactions between C<sub>60</sub> fullerene and Ala 25 and Glu 156 and Ile 27 and stacking and possible  $\pi$ -cation interaction of C<sub>60</sub> fullerene with Cys 153 and Asn 185, respectively. In turn, the gp91phox molecule is less flexible (1.2 Å). We believe that such flexibility of the gp91phox molecule is a reason for the significant displacement of C<sub>60</sub> fullerene (4.2 Å) and lack of its interaction with Lys 183 (average flexibility is

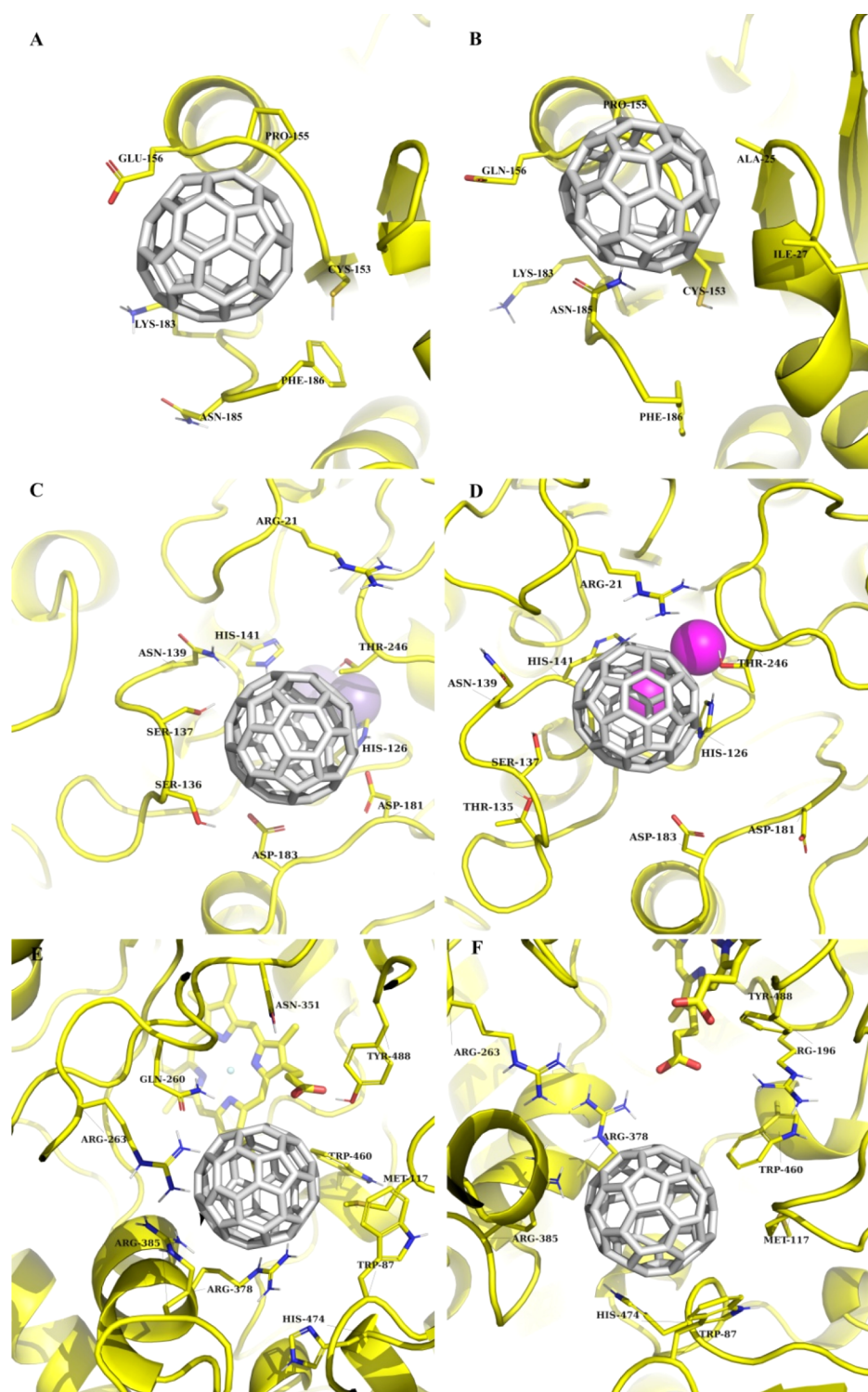


**Figure 1.** Results of molecular docking (left) and MD (right) simulations. Protein in yellow,  $C_{60}$  fullerene in gray. (A,B) gp91phox; (C,D) arginase; and (E,F) iNOS.

1.7 Å) and Phe 186 (average flexibility is 1.6 Å) comparing with molecular docking results (Figure 1).

Finally, the calculated Lennard-Jones short-range (LJ-SR) energy between gp91phox and  $C_{60}$  molecules in the complex is presented in Figure 3.

In the functional test, treatment of microglial cells with  $C_{60}$ FAS did not affect ROS generation (Figure 4). Dox used

alone caused the increase of ROS production. Complexation of Dox with  $C_{60}$  fullerene did not influence its pro-oxidant effect.

Nox2/gp91phox consists of a catalytic subunit, which is made up of an N-terminal transmembrane domain that binds two heme groups plus a C-terminal dehydrogenase domain that binds FAD and NADPH. Nox2/gp91phox binds to the small membrane-associated subunit p22phox, which both stabilize flavocytochrome and provide a binding site for

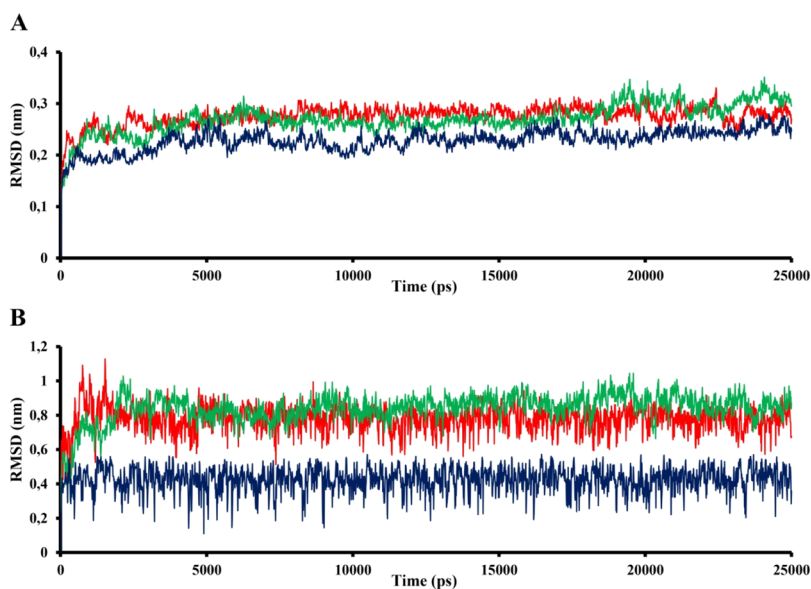


**Figure 2.** RMSD trajectories of obtained complexes. (A) protein, (B) C<sub>60</sub> fullerene. In red—gp91phox, green—arginase, and blue—iNOS.

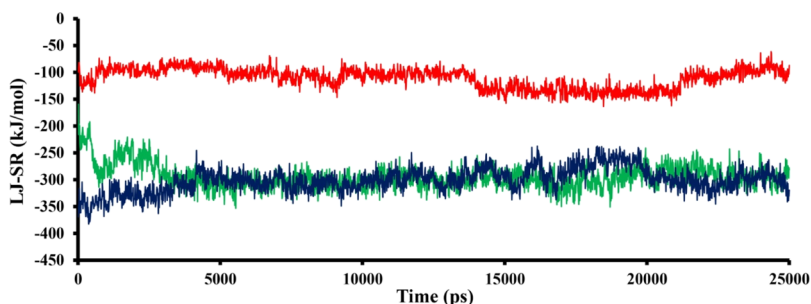


**Figure 3.** LJ-SR energy between the protein molecule and C<sub>60</sub> fullerene in the complex. In blue—gp91phox, green—arginase, and red—iNOS.

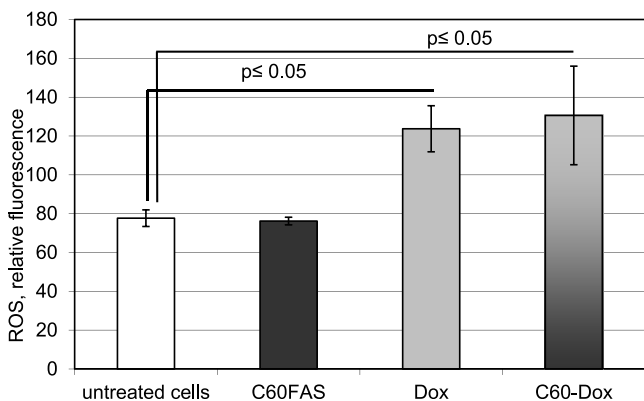


**Figure 4.** Effect of C<sub>60</sub>FAS, Dox, and C<sub>60</sub>-Dox nanocomplex on microglia ROS generation. Nonsensitized rat microglial cells were treated with nanoformulations for 30 min. ROS generation was examined by flow cytometry. Data are represented as mean ± SD for at least three independent experiments.

regulatory subunits (p47phox, p67phox, and small GTPase Rac). After assembly of the cytosolic regulatory subunits with membrane-associated gp91phox and p22phox, catalytic activity of NADPH oxidase starts off.<sup>67,68</sup> C<sub>60</sub> fullerene interacts with the structural part of gp91phox, which does not participate in the assembly of the enzymatic complex and catalytic activity of NADPH oxidase. Probably, this is one of the reasons of the

lack of the C<sub>60</sub> fullerene effect on microglia oxidative metabolism.

**Dox Complexation with C<sub>60</sub> Fullerene Interferes with its Stimulatory Effect on Microglia Phagocytic Activity.** Next, we examined the effect of C<sub>60</sub> fullerene and its nanocomplex with Dox on one of the crucial phagocyte functions—endocytic activity (phagocytosis). In our experiments, C<sub>60</sub>FAS did not influence phagocytic activity of resting nonsensitized microglial cells, neither the percentage of phagocytizing cells nor phagocytosis intensity (Figure 5).

Treatment with Dox resulted in substantial increase in the fraction of phagocytizing microglial cells and in the decrease of their phagocytosis intensity (Figure 5). In the nanocomplex with C<sub>60</sub> fullerene, Dox did not cause an increase of the fraction of phagocytizing microglial cells, but the PI of cells treated with the C<sub>60</sub>-Dox nanocomplex was significantly lower than that in control cells. Therefore, C<sub>60</sub> fullerene can partially diminish microglial cell phagocytosis activation caused by Dox.

**C<sub>60</sub> Fullerene Can Shift Microglia Arginine Metabolism.** Arginine metabolism is the most recognized criterium of functional polarization of both peripheral macrophages and microglia and is in the center of M1/M2 phagocyte dichotomy. Macrophages/microglia can metabolize arginine through arginase or iNOS. Arginase metabolizes arginine to ornithine and urea. Ornithine is a substrate for the synthesis of polyamines, polycationic molecules, which promote cell growth and tumor cell proliferation. In addition, arginase-

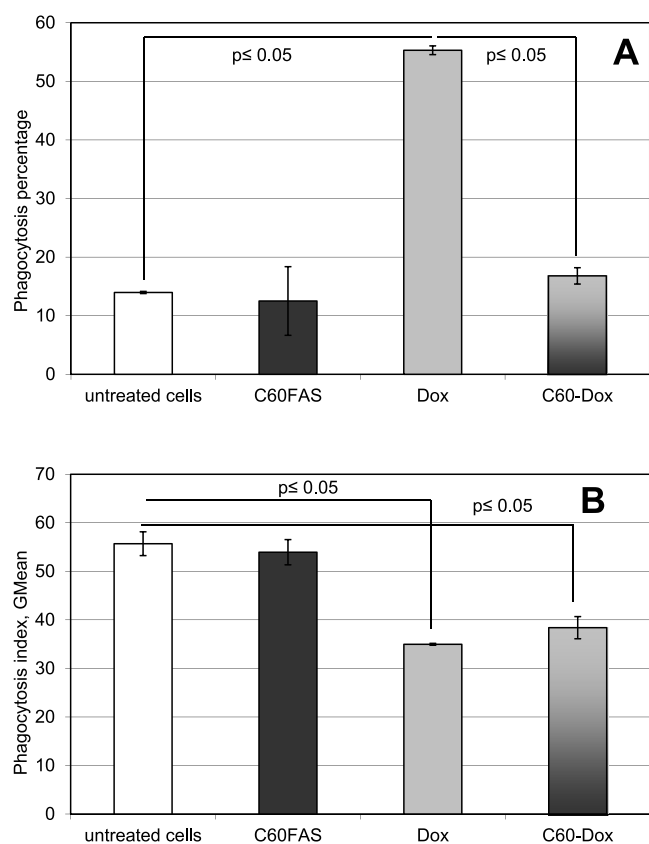


**Figure 5.** Effect of C<sub>60</sub>FAS, Dox, and C<sub>60</sub>-Dox nanocomplex on microglia phagocytic activity. Nonsensitized rat microglial cells were treated with nanoformulations for 30 min. Percentage of phagocytizing cells (A) and phagocytosis intensity (B) were determined by flow cytometry. Data are represented as mean  $\pm$  SD for at least three independent experiments.

derived ornithine is used for the production of proline, which is important in tissue remodeling processes, as well as fosters tumor invasive growth and metastasizing. Increased arginase activity is a marker of M2 macrophages/microglia. iNOS converts arginine to NO that is required for macrophage cytotoxic activity toward tumor cells. The shift of arginine metabolism toward increased iNOS activity is a sign of the macrophage/microglia M1 metabolic profile.<sup>69,70</sup>

**“Arginase–C<sub>60</sub> Fullerene” Complex.** According to molecular docking simulation, C<sub>60</sub> fullerene interacts in the *s*-2-(boronoethyl)-L-cysteine binding pocket, namely, it sterically bonds to Asp 181, Asp 183, Ser 136, Ser 137, and Thr 246. In turn, a much more impact on binding strength is caused by His 141 and His 126 (stacking interaction). Additionally, there is a possibility of  $\pi$ -cation interaction between C<sub>60</sub> fullerene and Arg 21. According to the structural biology of arginase, because of such interactions, C<sub>60</sub> fullerene blocks interaction of arginase with any other regulators of its functioning.<sup>71</sup> Furthermore, C<sub>60</sub> fullerene could create a strong  $\pi$ -cation interaction with two Mn<sup>2+</sup> atoms (locating inside the binding pocket) (Figure 1).

To investigate more deeply the “arginase–C<sub>60</sub> fullerene” interaction, MD simulation was performed. We parametrized Mn<sup>2+</sup> atoms accordingly.<sup>72</sup> During MD simulation, the obtained complex was stable. The movement ranges of arginase and C<sub>60</sub> fullerene are 0.11–0.35 and 0.28–1.04 nm, respectively (Figure 2). As it was expected after molecular docking, C<sub>60</sub> fullerene creates strong van der Waals forces with

His 126, His 141, and Arg 21. Besides, C<sub>60</sub> fullerene, despite its mobility, interacts strongly with two Mn<sup>2+</sup> atoms. We assume that such mobility is not related with displacement of C<sub>60</sub> fullerene and just only with its scrolling. The average distance between them within MD simulation is 0.5–0.8 nm. Note that the whole steric interactions determined in molecular docking simulation have been preserved (Figure 1).

**“iNOS–C<sub>60</sub> Fullerene” Complex.** The binding pocket of iNOS is located near the mesoheme structure. C<sub>60</sub> fullerene tightly stacks in the binding pocket and makes a huge amount of different interactions. So, it forms  $\pi$ -cation interactions with Arg 263, Arg 378, and Arg 385 and stacking interactions with Trp 87, Trp 460, His 474, and Met 117. In addition, C<sub>60</sub> fullerene potentially could create van der Waals force with Tyr 488 (Figure 1).

As a result of MD simulation, C<sub>60</sub> fullerene is characterized by less movement than proteins: C<sub>60</sub> fullerene is tightly clamped by van der Waals forces in the binding pocket (Figure 1); the movement of protein is in a similar range with the above described protein targets (Figure 2).

The calculated LJ-SR energies between the above protein molecules and C<sub>60</sub> fullerene in the appropriate complexes are presented in Figure 3.

Thus, computer simulation has revealed the possible stable “protein–C<sub>60</sub> fullerene” complexes for macrophage arginase and iNOS. Moreover, the C<sub>60</sub> fullerene binding site in iNOS is located within the oxygenase domain (amino acid residues 66  $\pm$  498), which plays a crucial role in substrate binding.<sup>73</sup> It suggests a potential regulatory effect of C<sub>60</sub> fullerene and its nanocomplex with Dox on iNOS activity. These results suggest a strong effect of C<sub>60</sub> fullerene on both microglia enzymes responsible for arginine metabolism and therefore for metabolic polarization.<sup>74</sup>

In our functional tests, C<sub>60</sub>FAS dramatically shifted microglia arginine metabolism to the decrease of NO-generation (Figure 6). These data correspond with our results which were obtained using circulating mononuclear phagocytes<sup>21</sup> and indicate that C<sub>60</sub>FAS per se promotes the activation of macrophage/microglia anti-inflammatory or the reparative metabolic program. Dox used alone did not significantly affect microglia arginine metabolism. At the same time, treatment of microglial cells with the C<sub>60</sub>-Dox nanocomplex resulted in a significant increase of their NO generation (Figure 6B). It indicates that C<sub>60</sub> fullerene can potentially facilitate the modulatory effect of Dox on the tumor microenvironment and thereby can augment its antitumor activity.

## DISCUSSION

Applications of nanoscale materials in neuroscience are only in the initial stages of development and require the investigation of the interaction of nanoparticles with different neural cells. Special interest is being given to the nanoformulation effect on microglia because these cells, like other tissue resident phagocytes, are the earliest and most sensitive responders to nanoparticles.

C<sub>60</sub> fullerenes have a wide range of applications in medicine as medicinal agents, diagnostic agents, imaging vectors, drug delivery vehicles, and so forth.<sup>75</sup> Their ability to cross the BBB makes C<sub>60</sub> fullerenes promising agents for the pharmacological therapy of neural disorders. The effect of C<sub>60</sub> fullerene on resident brain phagocytes—microglia—has not been explored yet.

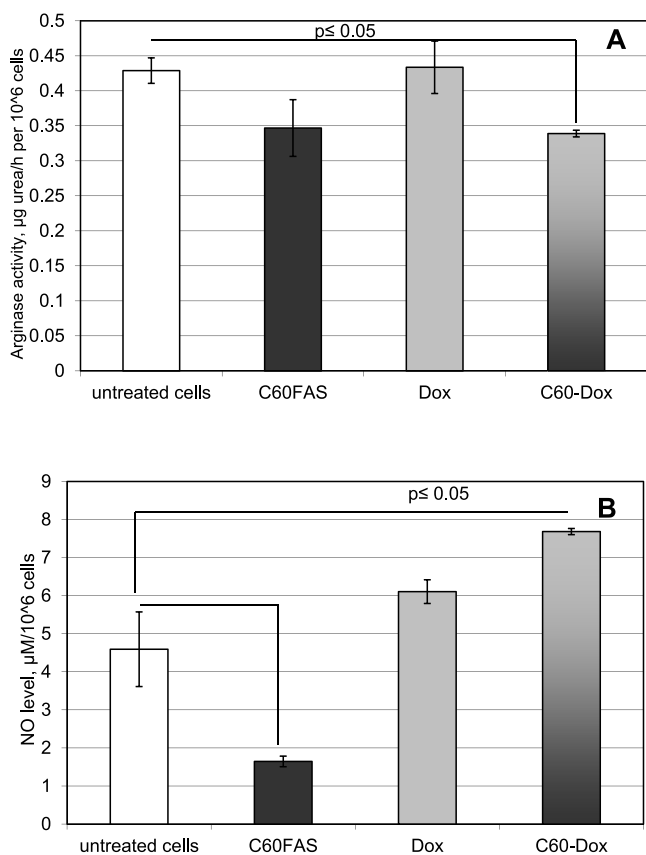


**Figure 6.** Effect of C<sub>60</sub>FAS, Dox, and C<sub>60</sub>-Dox nanocomplex on microglia arginine metabolism. Nonsensitized rat microglial cells were treated with nanoformulations for 30 min. Arginase activity (A) was examined in colorimetric assay. NO generation (B) was determined in Griess reaction. Data are represented as mean  $\pm$  SD of at least three independent experiments.

C<sub>60</sub> fullerenes and their nanocomplexes with pharmaceutical preparations can bind to different membrane receptors and intracellular receptive molecules expressed by phagocytes, including microglial cells.<sup>21,76</sup> Results of our previous experiments revealed that C<sub>60</sub> fullerenes and their nanocomplexes with Dox can exert membrane-dependent and direct intracellular effects on phagocyte functions such as ROS generation, phagocytosis, iNOS, and arginase activity.<sup>21</sup> All aforementioned phagocyte functional characteristics are inherent for microglial cells. However, a growing number of literature data shows unique microglial properties and functions, which differ these cells from the tissue-resident macrophages of any other location. It prompted us to explore the metabolic state of microglial cells after the exposition to C<sub>60</sub> fullerene and its nanocomplex with Dox.

As mentioned above, resting microglia exhibits a moderately M2-shifted phenotype. One of the major niche signals involved in such microglial maturation and functional polarization is TGF $\beta$ .<sup>77</sup> The M2-shifted metabolic profile of resident microglia plays dual role in the development of brain diseases. On the one hand, the M2-metabolic state allows microglia to maintain brain homeostasis efficiently and to restrain the development of neuroinflammation.<sup>78</sup> On the other hand, the M2-shifted functional state favors the accelerated development of tumor-associated microglia in the brain tumor microenvironment.<sup>79</sup> Results of our experiments also indicate slight M2-skew in the microglia metabolic profile as compared to

that in tissue-resident macrophages of another location—PMs. One can assume that it is one of the main reasons of differences in the response of microglia to the exposure to C<sub>60</sub> fullerene and its nanocomplex with Dox in comparison with that of circulating mononuclear phagocytes we observed in our previous experiments.<sup>21</sup>

As mentioned above, C<sub>60</sub> fullerenes and their derivatives can strongly affect phagocyte oxidative metabolism through the interaction with mitochondrial components and/or by binding to membrane pattern-recognizing receptors such as TLR4, and depending on the baseline state of the cell, they can stimulate or decrease ROS generation. Despite the fact that computer simulation revealed a stable interaction between C<sub>60</sub> fullerene and NOX2 (a component of the NADPH oxidase—the main source of ROS in tissue macrophages), the C<sub>60</sub> fullerene binding site is located out of the structural part influencing enzymatic activity of NADPH. It is one of the reasons why treatment of microglial cells with C<sub>60</sub>FAS did not affect ROS generation. The response of microglial cells to the exposure to C<sub>60</sub>FAS cardinaly differs from those of peripheral mononuclear phagocytes (a sharp increase of ROS generation in response to the exposure to C<sub>60</sub>FAS), which was observed in our previous experiments and was reported by other research groups.<sup>19–21,80</sup> As mentioned above, these differences might be caused by substantial distinctions in the transcriptional profile of microglia and peripheral phagocytes upon activation stipulated by functional features inherent to resident brain phagocytes.<sup>81</sup> It is widely reported that treatment-associated microglial ROS-generation is accompanied by notable neurotoxicity and complications such as cerebral edema and so forth.<sup>82</sup> Therefore, it might be especially important that we have found microglia showing no ROS-generating response to C<sub>60</sub>FAS. These results indicate C<sub>60</sub>FAS safety for nonsensitized microglial cells. Dox used alone caused the increase of ROS production, that is confirmed by the literature data.<sup>83</sup> Complexation of Dox with C<sub>60</sub> fullerene did not influence its pro-oxidant effect.

Microglial cells are the professional phagocytes of the brain. Of late years, the secretory profile and chemotactic activity of microglia have been well studied, whereas comparatively less consideration has been paid to microglia phagocytic activity. Whether upregulated microglial phagocytosis plays a beneficial or deleterious role in brain diseases remains debatable.<sup>84,85</sup> Effective clearance of apoptotic cells and tissue debris plays a crucial role for the neurogenesis and for the restoration of neuronal networking after acute brain injury as well as upon neurodegenerative disorders. It indicates that upregulated phagocytosis is a marker of microglia alternative (M2) polarization, which may be potentially protumoral.<sup>86</sup> On the other hand, in the tumor microenvironment, microglial cells exhibit capability to phagocytose tumor cells and, in such way, can participate in tumor growth retardation.<sup>87</sup> Whether microglial phagocytosis ensures as an anticancer defense or cancer-promoting mechanism still necessitates further study. In any case, initiation of phagocytic activity is a sign of microglial cell activation. In our experiments, C<sub>60</sub>FAS did not influence phagocytic activity of resting nonsensitized microglial cells, neither percentage of phagocytizing cells nor phagocytosis intensity. Such a reaction of microglial cells differs from that we observed in peripheral mononuclear phagocytes, where C<sub>60</sub>FAS caused phagocytosis enhancement. These data confirm once again the distinctive features of brain phagocyte activation in comparison with their peripheral counterparts.

Treatment with Dox resulted in substantial increase in the fraction of phagocytizing microglial cells and in the decrease of their phagocytosis intensity (Figure 5). It is well-known that Dox can trigger systemic inflammation. This inflammatory response is substantially mediated by the phagocyte activation including glial cells.<sup>88–90</sup> Our data also show the capacity of Dox to cause proinflammatory microglia activation. In the nanocomplex with C<sub>60</sub> fullerene, Dox did not cause an increase of the fraction of phagocytizing microglial cells, but the PI of cells treated with the C<sub>60</sub>–Dox nanocomplex was significantly lower than in control cells. How such changes in phagocytic activity will affect the overall metabolic profile of microglia is yet to be determined in subsequent experiments.

Arginine metabolism is the most validated marker for distinguishing M1 and M2 phagocytes. As mentioned above, M2-microglia with decreased NO-generation predominates in the brain tumor microenvironment. Elimination or re-education of these anti-inflammatory cells is reported to significantly reduce primary tumor growth and metastatic tumor burden.<sup>91,92</sup> The C<sub>60</sub>–Dox nanocomplex skews microglia arginine metabolism to a proinflammatory, tumor-suppressive profile and, in such a way, can potentiate the modulatory effect of chemotherapeutic drugs on the tumor microenvironment. On the other hand, M2 microglia activation facilitates neuroprotection and the resolution of neuroinflammation associated with neurodegeneration.<sup>93</sup> Our experiments demonstrated that C<sub>60</sub>FAS used alone shifts microglia arginine metabolism to the increase of arginase activity that indicates its anti-inflammatory effect.

## CONCLUSIONS

Collectively, our results show the modulatory effect of water-soluble pristine C<sub>60</sub> fullerene and its nanocomplex with Dox on microglial cells. C<sub>60</sub>FAS used alone exhibits only moderate action on the functions of resting microglia by skewing its arginine metabolism toward the anti-inflammatory profile. This makes C<sub>60</sub>FAS a promising agent for the correction of neuroinflammatory processes involved in neurodegeneration, and this deserves careful study in future experiments. In addition, the absence of toxic effects on resident brain phagocytes indicates a safety of C<sub>60</sub>FAS as a vehicle for drug delivery to the brain. Complexation of C<sub>60</sub> fullerene with Dox can potentiate tumoricidal properties of the latter by the activation of tumor-suppressive metabolic pathways in microglial cells.

## AUTHOR INFORMATION

### Corresponding Author

Mariia Rudyk – Taras Shevchenko National University of Kyiv, 01601 Kyiv, Ukraine; [orcid.org/0000-0003-1252-885X](https://orcid.org/0000-0003-1252-885X); Phone: +380504438775; Email: [rosiente@gmail.com](mailto:rosiente@gmail.com)

### Authors

Yevheniia Hurmach – Bogomolets National Medical University, 01601 Kyiv, Ukraine

Svitlana Prylutska – Taras Shevchenko National University of Kyiv, 01601 Kyiv, Ukraine

Vasyl Hurmach – Taras Shevchenko National University of Kyiv, 01601 Kyiv, Ukraine

Yuriy I. Prylutskyi – Taras Shevchenko National University of Kyiv, 01601 Kyiv, Ukraine

Uwe Ritter – Institute of Chemistry and Biotechnology, Technical University of Ilmenau, 98693 Ilmenau, Germany; [orcid.org/0000-0002-9315-4863](https://orcid.org/0000-0002-9315-4863)

Peter Scharff – Institute of Chemistry and Biotechnology, Technical University of Ilmenau, 98693 Ilmenau, Germany

Larysa Skivka – Taras Shevchenko National University of Kyiv, 01601 Kyiv, Ukraine

Complete contact information is available at:

<https://pubs.acs.org/10.1021/acs.molpharmaceut.0c00691>

## Notes

The authors declare no competing financial interest.

## ABBREVIATIONS

BBB, blood brain barrier; C<sub>60</sub>FAS, C<sub>60</sub> fullerene aqueous colloid solution; CNS, central nervous system; Dox, doxorubicin; FCS, fetal calf serum; FITC, fluorescein isothiocyanate; GR, Griess reagent; iNOS, inducible nitric oxide synthase; LJ-SR, Lennard-Jones energies short-range; MD, molecular dynamics; MFI, mean fluorescence intensity; NADPH, nicotinamide-adenine dinucleotide phosphate; NMR, nuclear magnetic resonance; NOX2, gp91phox; PBS, phosphate-buffered saline; PE, phycoerythrin; Phox, phagocyte NOX2; PI, phagocytosis index; PMs, peritoneal macrophages; rmsd, root mean square deviation; ROS, reactive oxygen species; Th1, T helper type 1; Th2, T helper type 2; TLR, toll-like receptor

## REFERENCES

- (1) Pampaloni, N. P.; Giugliano, M.; Scaini, D.; et al. Advances in nano neuroscience: from nanomaterials to nanotools. *Front. Neurosci.* **2019**, *12*, 953.
- (2) Yamago, S.; Tokuyama, H.; Nakamura, E.; et al. In vivo biological behavior of a water-miscible fullerene: <sup>14</sup>C labeling, absorption, distribution, excretion and acute toxicity. *Chem. Biol.* **1995**, *2*, 385–389.
- (3) Wu, Y.; Wang, R.; Wang, Y.; et al. Distinct impacts of fullerene on cognitive functions of dementia vs. non-dementia mice. *Neurotoxic. Res.* **2019**, *36*, 736–745.
- (4) Podolski, I. Y.; Poddubnaia, Z. A.; Godukhin, O. V. Fullerenes C<sub>60</sub>, anti-amyloid action, the brain, and cognitive processes. *Biofizika* **2010**, *55*, 71–76.
- (5) Zhu, X.; Sollogoub, M.; Zhang, Y. Biological applications of hydrophilic C<sub>60</sub> derivatives (hC<sub>60</sub>s)—a structural perspective. *Eur. J. Med. Chem.* **2016**, *115*, 438–452.
- (6) Prilutski, Y.; Durov, S.; Bulavin, L.; et al. Study of structure of colloidal particles of fullerenes in water solution. *Mol. Cryst. Liq. Cryst.* **1998**, *324*, 65–70.
- (7) Ritter, U.; Prylutskyi, Y. I.; Evstigneev, M. P.; et al. Structural features of highly stable reproducible C<sub>60</sub> fullerene aqueous colloid solution probed by various techniques. *Fullerenes, Nanotubes, Carbon Nanostruct.* **2015**, *23*, 530–534.
- (8) Levi, N.; Hantgan, R. R.; Lively, M. O.; et al. C<sub>60</sub>-fullerenes: detection of intracellular photoluminescence and lack of cytotoxic effects. *J. Nanobiotechnol.* **2006**, *4*, 14.
- (9) Prylutska, S. V.; Grebinyk, A. G.; Lynchak, O. V.; et al. In vitro and in vivo toxicity of pristine C<sub>60</sub> fullerene aqueous colloid solution. *Fullerenes, Nanotubes, Carbon Nanostruct.* **2019**, *27*, 715–728.
- (10) Sridhar, A.; Srikanth, B.; Kumar, A.; Dasmahapatra, A. K. Coarse-grain molecular dynamics study of fullerene transport across a cell membrane. *J. Chem. Phys.* **2015**, *143*, 024907.
- (11) Prylutskyi, Y.; Bychko, A.; Sokolova, V.; et al. Interaction of C<sub>60</sub> fullerene complexed to doxorubicin with model bilipid membranes and its uptake by HeLa cells. *Mater. Sci. Eng., C* **2016**, *59*, 398–403.

- (12) Shi, J.; Wang, B.; Wang, L.; et al. Fullerene (C<sub>60</sub>)-based tumor-targeting nanoparticles with “off-on” state for enhanced treatment of cancer. *J. Controlled Release* **2016**, *235*, 245–258.
- (13) Kumar, M.; Raza, K. C<sub>60</sub>-fullerenes as Drug Delivery Carriers for Anticancer Agents: Promises and Hurdles. *Pharm. Nanotechnol.* **2017**, *5*, 169–179.
- (14) Grebinyk, A.; Prylutska, S.; Grebinyk, S.; et al. Complexation with C<sub>60</sub> fullerene increases doxorubicin efficiency against leukemic cells in vitro. *Nanoscale Res. Lett.* **2019**, *14*, 61.
- (15) Prylutska, S.; Grynyuk, I.; Skaterna, T.; et al. Toxicity of C<sub>60</sub> fullerene-cisplatin nanocomplex against Lewis lung carcinoma cells. *Arch. Toxicol.* **2019**, *93*, 1213–1226.
- (16) Elshater, A.-E. A.; Haridy, M. A. M.; Salman, M. M. A.; et al. Fullerene C<sub>60</sub> nanoparticles ameliorated cyclophosphamide-induced acute hepatotoxicity in rats. *Biomed. Pharmacother.* **2018**, *97*, 53–59.
- (17) Johnston, H. J.; Hutchison, G. R.; Christensen, F. M.; et al. The biological mechanisms and physicochemical characteristics responsible for driving fullerene toxicity. *Toxicol. Sci.* **2010**, *114*, 162–182.
- (18) Russ, K. A.; Elvati, P.; Parsonage, T. L.; et al. C<sub>60</sub> fullerene localization and membrane interactions in RAW 264.7 immortalized mouse macrophages. *Nanoscale* **2016**, *8*, 4134–4144.
- (19) Xiang, K.; Dou, Z.; Li, Y.; et al. Cytotoxicity and TNF- $\alpha$  secretion in RAW264.7 macrophages exposed to different fullerene derivatives. *J. Nanosci. Nanotechnol.* **2012**, *12*, 2169–2178.
- (20) Santos, S. M.; Dinis, A. M.; Peixoto, F.; et al. Interaction of fullerene nanoparticles with biomembranes: from the partition in lipid membranes to effects on mitochondrial bioenergetics. *Toxicol. Sci.* **2014**, *138*, 117–129.
- (21) Skivka, L. M.; Prylutska, S. V.; Rudyk, M. P.; et al. C<sub>60</sub> fullerene and its nanocomplexes with anticancer drugs modulate circulating phagocyte functions and dramatically increase ROS generation in transformed monocytes. *Cancer Nanotechnol.* **2018**, *9*, 8.
- (22) Caputa, G.; Castoldi, A.; Pearce, E. J. Metabolic adaptations of tissue-resident immune cells. *Nat. Immunol.* **2019**, *20*, 793–801.
- (23) T’Jonck, W.; Guillems, M.; Bonnardel, J. Niche signals and transcription factors involved in tissue-resident macrophage development. *Cell. Immunol.* **2018**, *330*, 43–53.
- (24) Masuda, T.; Prinz, M. Microglia: a unique versatile cell in the central nervous system. *ACS Chem. Neurosci.* **2016**, *7*, 428–434.
- (25) Sousa, C.; Biber, K.; Michelucci, A. Cellular and molecular characterization of microglia: a unique immune cell population. *Front. Immunol.* **2017**, *8*, 198.
- (26) Tsui, C.; Koss, K.; Churchward, M. A.; Todd, K. G. Biomaterials and glia: Progress on designs to modulate neuro-inflammation. *Acta Biomater.* **2019**, *83*, 13–28.
- (27) Sica, A.; Erreni, M.; Allavena, P.; et al. Macrophage polarization in pathology. *Cell. Mol. Life Sci.* **2015**, *72*, 4111–4126.
- (28) Murray, P. J. Macrophage polarization. *Annu. Rev. Physiol.* **2017**, *79*, 541–566.
- (29) Cherry, J. D.; Olschowka, J. A.; O’Banion, M. K. Are “resting” microglia more “m2”? *Front. Immunol.* **2014**, *5*, 594.
- (30) Ransohoff, R. M. A polarizing question: do M1 and M2 microglia exist? *Nat. Neurosci.* **2016**, *19*, 987–991.
- (31) Ye, S.; Zhou, T.; Cheng, K.; et al. Carboxylic Acid Fullerene (C<sub>60</sub>) Derivatives Attenuated Neuroinflammatory Responses by Modulating Mitochondrial Dynamics. *Nanoscale Res. Lett.* **2015**, *10*, 246.
- (32) Maysinger, D.; Zhang, I. Nutritional and nanotechnological modulators of microglia. *Front. Immunol.* **2016**, *7*, 270.
- (33) Fiorito, S.; Russier, J.; Salemme, A.; et al. Switching on microglia with electro-conductive multi walled carbon nanotubes. *Carbon* **2018**, *129*, 572–584.
- (34) Li, T.-F.; Li, K.; Wang, C.; et al. Harnessing the cross-talk between tumor cells and tumor-associated macrophages with a nano-drug for modulation of glioblastoma immune microenvironment. *J. Controlled Release* **2017**, *268*, 128–146.
- (35) Prylutsky, Y.I.; Evstigneev, M. P.; Cherepanov, V. V.; et al. Structural organization of C<sub>60</sub> fullerene, doxorubicin and their complex in physiological solution as promising antitumor agents. *J. Nanopart. Res.* **2015**, *17*, 45–49.
- (36) Prylutsky, Y. I.; Evstigneev, M. P.; Pashkova, I. S.; et al. Characterization of C<sub>60</sub> fullerene complexation with antibiotic doxorubicin. *Phys. Chem. Chem. Phys.* **2014**, *16*, 23164–23172.
- (37) Prylutsky, Y.; Borowik, A.; Goluński, G.; et al. Biophysical characterization of the complexation of C<sub>60</sub> fullerene with doxorubicin in a prokaryotic model. *Materialwiss. Werkstofftech.* **2016**, *47*, 92–97.
- (38) Mosunov, A. A.; Pashkova, I. S.; Sidorova, M.; et al. Determination of equilibrium constant of C<sub>60</sub> fullerene binding with drug molecules. *Phys. Chem. Chem. Phys.* **2017**, *19*, 6777–6784.
- (39) Grebinyk, A.; Prylutska, S.; Chepurina, O.; et al. Synergy of chemo- and photodynamic therapies with C<sub>60</sub> fullerene-doxorubicin nanocomplex. *Nanomaterials* **2019**, *9*, 1540.
- (40) Waterhouse, A.; Bertoni, M.; Bienert, S.; et al. SWISS-MODEL: homology modelling of protein structures and complexes. *Nucleic Acids Res.* **2018**, *46*, W296–W303.
- (41) Bienert, S.; Waterhouse, A.; de Beer, T. A. P.; et al. The SWISS-MODEL Repository—new features and functionality. *Nucleic Acids Res.* **2017**, *45*, D313–D319.
- (42) Guex, N.; Peitsch, M. C.; Schwede, T. Automated comparative protein structure modeling with SWISS-MODEL and Swiss-PdbViewer: A historical perspective. *Electrophoresis* **2009**, *30*, S162–S173.
- (43) Benkert, P.; Biasini, M.; Schwede, T. Toward the estimation of the absolute quality of individual protein structure models. *Bioinformatics* **2011**, *27*, 343–350.
- (44) Bertoni, M.; Kiefer, F.; Biasini, M.; et al. Modeling protein quaternary structure of homo- and hetero-oligomers beyond binary interactions by homology. *Sci. Rep.* **2017**, *7*, 10480.
- (45) Warren, G. L.; Andrews, C. W.; Capelli, A.-M.; et al. A critical assessment of docking programs and scoring functions. *J. Med. Chem.* **2006**, *49*, 5912–5931.
- (46) McMartin, C.; Bohacek, R. S. QXP: powerful, rapid computer algorithms for structure-based drug design. *J. Comput.-Aided Mol. Des.* **1997**, *11*, 333–344.
- (47) Abraham, M. J.; Murtola, T.; Schulz, R.; et al. GROMACS: High performance molecular simulations through multi-level parallelism from laptops to supercomputers. *SoftwareX* **2015**, *1–2*, 19–25.
- (48) Huang, J.; MacKerell, A. D. CHARMM36 all-atom additive protein force field: validation based on comparison to NMR data. *J. Comput. Chem.* **2013**, *34*, 2135–2145.
- (49) Zoete, V.; Cuendet, M. A.; Grosdidier, A.; Michielin, O. SwissParam, a Fast Force Field Generation Tool For Small Organic Molecules. *J. Comput. Chem.* **2011**, *32*, 2359–2368.
- (50) Frank, M. G.; Wieseler-Frank, J. L.; Watkins, L. R.; Maier, S. F. Rapid isolation of highly enriched and quiescent microglia from adult rat hippocampus: Immunophenotypic and functional characteristics. *J. Neurosci. Methods* **2006**, *151*, 121–130.
- (51) Skivka, L. M.; Fedorchuk, O. G.; Rudyk, M. P.; et al. Antineoplastic drug NSC631570 modulates functions of hypoxic macrophages. *Cytol. Genet.* **2013**, *47*, 318–328.
- (52) Reiner, N. E. *Macrophages and Dendritic Cells: Methods and Protocols*; Humana Press: New York, 2009; pp 29–45.
- (53) Cantinieaux, B.; Hariga, C.; Courtoy, P.; et al. Staphylococcus aureus phagocytosis. A new cytofluorometric method using FITC and paraformaldehyde. *J. Immunol. Methods* **1989**, *121*, 203–208.
- (54) Hurmach, Y.; Rudyk, M.; Svyatetska, V.; et al. The effect of intranasally administered TLR3 agonist larifan on metabolic profile of microglial cells in rat with C6 glioma. *Ukr. Biochem. J.* **2018**, *90*, 110–119.
- (55) Feito, M. J.; Diez-Orejas, R.; Cicuéndez, M.; et al. Characterization of M1 and M2 polarization phenotypes in peritoneal macrophages after treatment with graphene oxide nanosheets. *Colloids Surf., B* **2019**, *176*, 96–105.
- (56) Xu, Z.-J.; Gu, Y.; Wang, C.-Z.; et al. The M2 macrophage marker CD206: a novel prognostic indicator for acute myeloid leukemia. *Oncoimmunology* **2020**, *9*, 1683347.

- (57) Hellström Erkenstam, N.; Smith, P. L.; Fleiss, B.; et al. Temporal characterization of microglia/macrophage phenotypes in a mouse model of neonatal hypoxic-ischemic brain injury. *Front. Cell. Neurosci.* **2016**, *10*, 286.
- (58) Zhao, Y.-L.; Tian, P.-x.; Han, F.; et al. Comparison of the characteristics of macrophages derived from murine spleen, peritoneal cavity, and bone marrow. *J. Zhejiang Univ., Sci., B* **2017**, *18*, 1055–1063.
- (59) Oishi, S.; Takano, R.; Tamura, S.; et al. M2 polarization of murine peritoneal macrophages induces regulatory cytokine production and suppresses T-cell proliferation. *Immunology* **2016**, *149*, 320–328.
- (60) Foley, S.; Crowley, C.; Smaih, M.; et al. Cellular localisation of a water-soluble fullerene derivative. *Biochem. Biophys. Res. Commun.* **2002**, *294*, 116–119.
- (61) Gharbi, N.; Pressac, M.; Hadchouel, M.; et al. [60] fullerene is a powerful antioxidant in vivo with no acute or subacute toxicity. *Nano Lett.* **2005**, *5*, 2578–2585.
- (62) Dellinger, A.; Zhou, Z.; Connor, J.; et al. Application of fullerenes in nanomedicine: an update. *Nanomedicine* **2013**, *8*, 1191–1208.
- (63) Bae, Y. S.; Lee, J. H.; Choi, S. H.; et al. Macrophages generate reactive oxygen species in response to minimally oxidized low-density lipoprotein: toll-like receptor 4- and spleen tyrosine kinase-dependent activation of NADPH oxidase 2. *Circ. Res.* **2009**, *104*, 210–218.
- (64) Dohi, K.; Ohtaki, H.; Nakamachi, T.; et al. Gp91phox (NOX2) in classically activated microglia exacerbates traumatic brain injury. *J. Neuroinflammation* **2010**, *7*, 41.
- (65) Lambeth, J. D.; Neish, A. S. Nox enzymes and new thinking on reactive oxygen: a double-edged sword revisited. *Annu. Rev. Pathol.: Mech. Dis.* **2014**, *9*, 119–145.
- (66) Joo, J. H.; Huh, J.-E.; Lee, J. H.; et al. A novel pyrazole derivative protects from ovariectomy-induced osteoporosis through the inhibition of NADPH oxidase. *Sci. Rep.* **2016**, *6*, 22389.
- (67) Aguirre, J.; Lambeth, J. D. Nox enzymes from fungus to fly to fish and what they tell us about Nox function in mammals. *Free Radical Biol. Med.* **2010**, *49*, 1342–1353.
- (68) Panday, A.; Sahoo, M. K.; Osorio, D.; Batra, S. NADPH oxidases: an overview from structure to innate immunity-associated pathologies. *Cell. Mol. Immunol.* **2015**, *12*, 5–23.
- (69) Rath, M.; Müller, I.; Kropf, P.; et al. Metabolism via Arginase or Nitric Oxide Synthase: Two Competing Arginine Pathways in Macrophages. *Front. Immunol.* **2014**, *5*, 532.
- (70) Pekarova, M.; Lojek, A. The crucial role of l-arginine in macrophage activation: What you need to know about it. *Life Sci.* **2015**, *137*, 44–48.
- (71) Di Costanzo, L.; Sabio, G.; Mora, A.; et al. Crystal structure of human arginase I at 1.29-Å resolution and exploration of inhibition in the immune response. *Proc. Natl. Acad. Sci. U.S.A.* **2005**, *102*, 13058–13063.
- (72) Won, Y. Force Field for Monovalent, Divalent, and Trivalent Cations Developed under the Solvent Boundary Potential. *J. Phys. Chem. A* **2012**, *116*, 11763–11767.
- (73) Alderton, W. K.; Cooper, C. E.; Knowles, R. G. Nitric oxide synthases: structure, function and inhibition. *Biochem. J.* **2001**, *357*, 593–615.
- (74) Zhang, I.; Alizadeh, D.; Liang, J.; et al. Characterization of arginase expression in glioma-associated microglia and macrophages. *PLoS One* **2016**, *11*, No. e0165118.
- (75) Lin, C.-M.; Lu, T.-Y. C60 fullerene derivatized nanoparticles and their application to therapeutics. *Recent Pat. Nanotechnol.* **2012**, *6*, 105–113.
- (76) Turabekova, M.; Rasulev, B.; Theodore, M.; et al. Immunotoxicity of nanoparticles: a computational study suggests that CNTs and C60 fullerenes might be recognized as pathogens by Toll-like receptors. *Nanoscale* **2014**, *6*, 3488–3495.
- (77) Zöllner, T.; Schneider, A.; Kleimeyer, C.; et al. Silencing of TGF $\beta$  signalling in microglia results in impaired homeostasis. *Nat. Commun.* **2018**, *9*, 4011.
- (78) Song, Y.; Li, Z.; He, T.; et al. M2 microglia-derived exosomes protect the mouse brain from ischemia-reperfusion injury via exosomal miR-124. *Theranostics* **2019**, *9*, 2910–2923.
- (79) Morisse, M. C.; Jouannet, S.; Dominguez-Villar, M.; et al. Interactions between tumor-associated macrophages and tumor cells in glioblastoma: unraveling promising targeted therapies. *Expert Rev. Neurother.* **2018**, *18*, 729–737.
- (80) Vesnina, L. É.; Mamontova, T. V.; Mikitiuk, M. V.; et al. Effect of fullerene C60 on functional activity of phagocytic cells. *Eksp. Klin. Farmakol.* **2011**, *74*, 26–29.
- (81) Hutter, G.; Theruvath, J.; Graef, C. M.; et al. Microglia are effector cells of CD47-SIRP $\alpha$  antiphagocytic axis disruption against glioblastoma. *Proc. Natl. Acad. Sci. U.S.A.* **2019**, *116*, 997–1006.
- (82) Brown, G. C.; Vilalta, A. How microglia kill neurons. *Brain Res.* **2015**, *1628*, 288–297.
- (83) Keeney, J. T. R.; Miriyala, S.; Noel, T.; et al. Superoxide induces protein oxidation in plasma and TNF- $\alpha$  elevation in macrophage culture: Insights into mechanisms of neurotoxicity following doxorubicin chemotherapy. *Cancer Lett.* **2015**, *367*, 157–161.
- (84) Wolf, S. A.; Boddeke, H. W. G. M.; Kettenmann, H. Microglia in physiology and disease. *Annu. Rev. Physiol.* **2017**, *79*, 619–643.
- (85) Fu, R.; Shen, Q.; Xu, P.; et al. Phagocytosis of microglia in the central nervous system diseases. *Mol. Neurobiol.* **2014**, *49*, 1422–1434.
- (86) Sierra, A.; Encinas, J. M.; Deudero, J. J. P.; Chancey, J. H.; Enikolopov, G.; Overstreet-Wadiche, L. S.; Tsirka, S. E.; Maletic-Savatic, M. Microglia shape adult hippocampal neurogenesis through apoptosis-coupled phagocytosis. *Cell Stem Cell* **2010**, *7*, 483–495.
- (87) Chang, G. H.-F.; Barbaro, N. M.; Pieper, R. O. Phosphatidylserine-dependent phagocytosis of apoptotic glioma cells by normal human microglia, astrocytes, and glioma cells. *J. Neuro-Oncol.* **2000**, *2*, 174–183.
- (88) Sauter, K. A. D.; Wood, L. J.; Wong, J.; et al. Doxorubicin and daunorubicin induce processing and release of interleukin-1 $\beta$  through activation of the NLRP3 inflammasome. *Cancer Biol. Ther.* **2011**, *11*, 1008–1016.
- (89) Wang, L.; Chen, Q.; Qi, H.; et al. Doxorubicin-induced systemic inflammation is driven by upregulation of Toll-like receptor TLR4 and endotoxin leakage. *Cancer Res.* **2016**, *76*, 6631–6642.
- (90) Siswanto, S.; Arozal, W.; Juniantito, V.; et al. The effect of mangiferin against brain damage caused by oxidative stress and inflammation induced by doxorubicin. *HAYATI J Biosci* **2016**, *23*, 51–55.
- (91) Zhang, H.; Zhang, W.; Sun, X.; et al. Class A1 scavenger receptor modulates glioma progression by regulating M2-like tumor-associated macrophage polarization. *Oncotarget* **2016**, *7*, 50099–50116.
- (92) Andreou, K. E.; Soto, M. S.; Allen, D.; et al. Anti-inflammatory microglia/macrophages as a potential therapeutic target in brain metastasis. *Front. Radiat. Oncol.* **2017**, *7*, 251.
- (93) Du, L.; Zhang, Y.; Chen, Y.; et al. Role of microglia in neurological disorders and their potentials as a therapeutic target. *Mol. Neurobiol.* **2017**, *54*, 7567–7584.